# Revealing metabolic storage processes in electrode respiring bacteria by differential electrochemical mass spectrometry

F. Kubannek[a], U. Schröder[b], U. Krewer[a,*]

[a] *Institute of Energy and Process Systems Engineering, Technische Universität Braunschweig, Franz-Liszt-Str. 35, Braunschweig, Germany*
[b] *Institute of Environmental and Sustainable Chemistry, Technische Universität Braunschweig, Hagenring 30, Braunschweig, Germany*

ARTICLE INFO

*Keywords:*
Microbial fuel cell
Charge and carbon storage
Online measurement of $CO_2$ production
Differential electrochemical mass spectrometry
Mass spectrometric cyclic voltammetry

ABSTRACT

In this work we employ differential electrochemical mass spectrometry (DEMS) in combination with static and dynamic electrochemical techniques for the study of metabolic processes of electrochemically active bacteria. $CO_2$ production during acetate oxidation by electrode respiring bacteria was measured, in-vivo and online with a sensitivity of $6.5 \cdot 10^{-13}$ mol/s. The correlation of ion current and electrical current provides insight into the interaction of metabolic processes and extra-cellular electron transfer. In low-turnover CVs, two competing potential dependent electron transfer mechanisms were observed and formal potentials of two redox systems that are involved in complete oxidation of acetate to $CO_2$ were determined. By balancing charge and carbon flows during dynamic measurements, two significant storage mechanisms in electrochemically active bacteria were identified: 1) a charge storage mechanism that allows substrate oxidation to proceed at a constant rate despite of external current flowing in cathodic direction. 2) a carbon storage mechanism that allows the biofilm to take up acetate at an unchanged rate at very low potentials even though the oxidation to $CO_2$ stops. These storage capabilities allow a limited decoupling of electrical current and $CO_2$ production rate.

## 1. Introduction

Gaining deeper knowledge on electron transfer mechanisms and energy conversion in bioelectrochemical systems (BES) is not only of scientific interest but also highly relevant for system design for technical applications. In most BES, anode respiring bacteria (ARB) form a biofilm that is firmly attached to a solid electrode. There are numerous in-situ and ex-situ techniques for studying ARB [1] but most of them focus on the transfer of electrons out of the cell to an electrode. Analysis of metabolic processes in the cell are usually not conducted online, but rather ex-situ [2]. They also require to irreversibly destroy the biofilm. Dynamic techniques are non-destructive and allow to study the interaction of transport processes and kinetics by evaluating typical response signals [3]: Chronoamperometry, impedance spectroscopy and cyclic voltammetry have been used extensively to characterize, analyse, and even improve the oxidation of C-containing fuels; they may be combined with surface and concentration measurements such as mass spectrometry and infrared spectroscopy to obtain further insights [3]. One of the most popular dynamic techniques for studying phenomena related to extracellular electron transfer (EET) between a biofilm and an electrode is cyclic voltammetry (CV). Usually two types of CVs are distinguished in the field of BES [4]: non-turnover and turnover CVs. Non-turnover CVs are recorded using substrate-depleted solutions, i.e. at conditions where there is no substrate available to the biofilm. The current recorded then is only due to capacitive effects and due to the oxidation and reduction of redox systems within the cell. When no substrate oxidation or other irreversible processes take place, the integrals of positive and negative currents over time are equal and the average current is zero. The peaks observed in the CV can be assigned to certain redox systems such as the outer membrane protein OmcB [4,5]. However, as no substrate oxidation takes place under non-turnover conditions, assigning oxidation and reduction of these redox systems to processes observed in the substrate metabolizing biofilm needs to be done with uttermost care. On the other hand, turnover CVs are recorded at high substrate availability. The measured current mainly results from substrate oxidation and often follows an s-shaped curve [4,6,7]. Since substrate oxidation is irreversible, the average current under turnover-conditions is usually

* Corresponding author.
*E-mail addresses:* f.kubannek@tu-braunschweig.de (F. Kubannek), uwe.schroeder@tu-braunschweig.de (U. Schröder), u.krewer@tu-braunschweig.de (U. Krewer).

positive. Current peaks from oxidation and reduction of inter-cellular redox systems are masked by the large current from substrate oxidation. Thus, it is difficult to clearly identify the role that each redox system plays in substrate oxidation from turnover as well as from non-turnover CVs.

Direct, non-invasive measurement of metabolites or products such as $CO_2$ during CVs would help to understand the contributions of the redox systems that are visible in CVs to anodic respiration. So far, measurements of gas production in microbial fuel cells or electrolysis cells have been limited to headspace gas analysis by gas chromatography and quantification by measuring the total volume of collected gas [8–10]. The reported approaches did not achieve the time resolution needed to monitor product formation during CV measurements. One reason is that the equilibrium reaction between hydrogen carbonate and $CO_2$ slows down the transfer of $CO_2$ from a buffered solution near pH 7 into the gas phase [11] so that even small headspace volumes and intense stirring are unlikely to solve this problem. An alternative technique applied for non-electrochemical reactions is membrane inlet mass spectrometry (MIMS); with this technique, volatile products and intermediates from normal bacteria have been analysed online [12,13]. MIMS yields a high time resolution and sensitivity because volatile substances pervaporate through a gas-permeable membrane into a vacuum system where they are detected by mass spectrometry. It has already been shown that $CO_2$ production in bioreactors can be monitored and quantified this way [11,14]. Following these studies, we suggest the use of differential electrochemical mass spectrometry (DEMS) in combination with static and dynamic electrochemical techniques for the study of metabolic processes of electrochemically active bacteria. While DEMS has been numerously used to study electrode reactions [15,16], so far no bioelectrochemical reactions have been investigated by DEMS. During DEMS measurements, volatile products and intermediates of electrochemical reactions pervaporate through a PTFE membrane into a differentially pumped vacuum system where they are detected by mass spectrometry. The membrane is placed closely to the electrode to minimize time delays. This online-technique provides a high sensitivity, short response times, and allows quantification. In a recent study, we combined quantitative DEMS experiments and modelling of electrochemical reactions to analyse kinetics of CO oxidation at porous electrodes [17].

Further information on DEMS can be found for instance in two comprehensive reviews by Baltruschat and co-workers [15,16].

In this work we combine DEMS with cyclic voltammetry of electroactive anodic biofilms for the first time. Mass spectrometric cyclic voltammograms ( MSCVs) that allow to directly correlate $CO_2$ production and current at high and low substrate availability are reported, and electron transfer systems that are related to $CO_2$ production are identified. We demonstrate that DEMS can be employed for quantitative analysis of the $CO_2$ production rate of electrochemically active bacteria and discuss two intra-cellular storage mechanisms for charge and substrate as well as their implications on the analysis of BES.

## 2. Experimental

### 2.1. Electrochemical cell

The experiments were conducted in the cyclone flow DEMS cell which we described and characterized in detail earlier [17]. In brief, a working electrode made from PTFE-free carbon paper ($r = 0.5$ cm, $d = 0.2$ mm, Sigracet GDL 29AA) is mounted at the bottom of a cyclone flow cell that allows to establish defined mass transfer conditions at the electrode. A porous PTFE membrane (Pall Membranes, specified pore size 0.2 µm, thickness 60 µm) is pressed against the bottom of the working electrode separating the working electrode compartment from the mass spectrometer's vacuum system. Through this membrane, volatile substances evaporate into the vacuum where they are detected by a mass spectrometer (Pfeiffer QMG220 M1 quadropole mass spectrometer with secondary ion multiplier). Because of the direct contact of electrode and membrane, volatile species have a short diffusion path into the vacuum system. The ion current at a mass to charge ratio of $m/z = 44$ ($CO_2$) was recorded throughout the duration of the experiment. The complete setup is depicted in Schematic 1: A peristaltic pump recirculated the substrate solution from the cyclone cell to a glass vessel at 105 ml min$^{-1}$. This vessel was constantly purged with high purity nitrogen (99.999% Westfalen AG) in order to remove oxygen and to prevent the accumulation of volatile substances in the bulk solution. The volume of the flow cell is 77 ml, the total liquid volume including the recirculation vessel and the tubing is approximately 160 ml. FEP (fluorinated ethylene propylene) tubing was chosen as a compromise between chemical inertness and gas permeability.

The temperature in the recirculation vessel was kept at 36 °C, resulting in a temperature of 35 °C in the working electrode compartment. The calibration of the MS with $CO_2$ (99.999%, Westfalen AG) was done as described elsewhere [17].

A saturated Silver/Silver-Chloride electrode was used as a reference electrode. The counter electrode was made from a platinum wire. It was placed at the outlet of the cyclone cell and separated from the cell volume by a glass frit.

### 2.2. Electrochemical measurements

A Gamry Reference 3000 potentiostat was used for electrochemical measurements. All potentials are reported with respect to the saturated Silver/Silver-Chloride Reference Electrode (Meinsberger Elektroden, Germany, +0.197 V vs. SHE). Chronoamperometry (CA) was recorded at a constant potential of 0.2 V, cyclic voltammograms (CV) were recorded from 0.2 V to −0.5 V at the scan rates given below. Two cycles were recorded, they showed only minor deviations. For all CVs, the second cycle is shown. Also potential steps from 0.2 V to −0.5 V and back to 0.2 V were applied.

### 2.3. Inoculum and media composition

The inoculum was a mixed culture biofilm scraped from an secondary biofilm electrode. No further analysis of the biofilm population was conducted. However, a community analysis was conducted in another recent study [18], where we used waste water from the same source (Wastewater treatment plant Steinhof, Braunschweig, Germany) as initial inoculum, and applied the same growth conditions and cultivation steps. There the biofilm consisted mainly of *Geobacter anodireducens*. Because of the very similar culturing

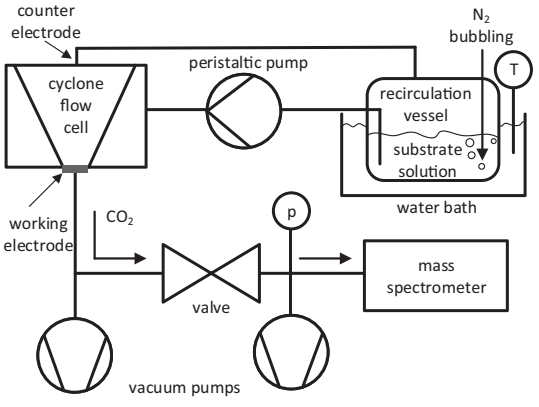


**Schematic 1.** Experimental setup including DEMS, cyclone flow cell, and substrate recirculation loop.

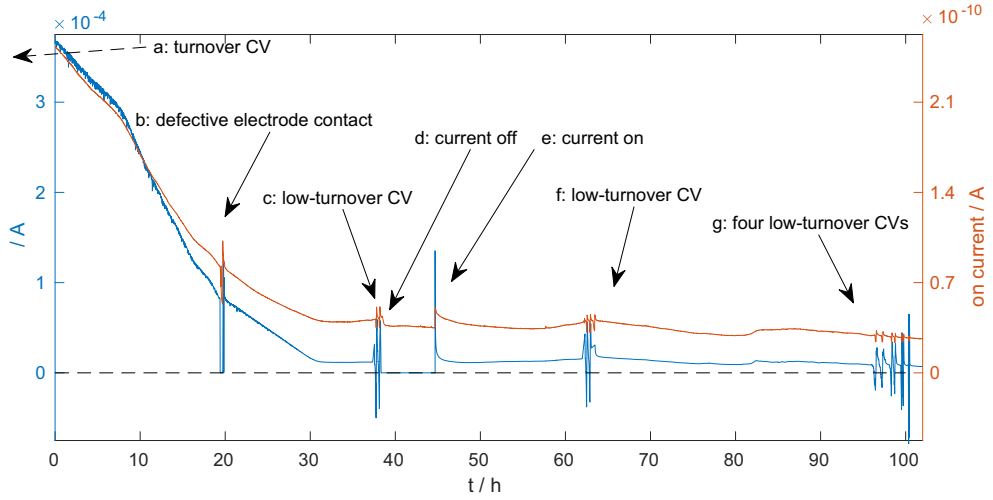


**Fig. 1.** Current and ion current at $m/z = 44$ over time. Potential is 0.2 V except for the points indicated by the arrows. a: turnover CV (recorded 30 h before the data series shown in this figure), b: defective electrode contact (open circuit condition), c: CV one, d: CA interrupted (open circuit condition), e: CA restarted, f: CV two, g: CVs three to six. Ion current is potted in orange, electrode current in blue. (For interpretation of the references to color in this figure legend, the reader is referred to the web version of this article.)

conditions, it seems likely that *G. anodireducens* also contributed significantly to the biofilm in this study. Based on previous studies, we also attribute the reddish color of the biofilm and the shape of non-turnover CVs (see also Section 3.2) to a high share of *Geobacter* species [4,19,20].

The substrate solution was prepared with ultrapure water (Millipore Milli-Q 18.2 MΩ cm). 1 L of substrate solution contained 10 mmol sodium acetate, 2.69 g $NaH_2PO_4$, 4.33 g $Na_2HPO_4$, 0.31 g $NH_4Cl$, 0.31 g KCl [21], 12.5 ml trace element solution and 12.5 ml vitamin solution [22]. After inoculation, three batch cycles were performed in order to reach stationary biofilm conditions. In the beginning of each batch cycle, the cyclone cell and the recirculation vessel were filled with fresh de-aerated substrate solution. During the batch cycles, no additional substrate was added so that the substrate concentration was continuously decreasing throughout the cycle. The CV discussed in this work were recorded in the last phase of the third batch cycle. Therefore results are valid for a stable biofilm that does not change its properties due to biofilm growth. The cell was connected to the vacuum system and the mass spectrometer only in the third cycle.

## 3. Results and discussion

### 3.1. Chronoamperometry

In Fig. 1, the development of current and ion current for $CO_2$ at $m/z = 44$ over time are depicted for the last phase of the third batch cycle. The potential of the working electrode is 0.2 V throughout the experiments except for the points marked *a* to *g* which will be discussed in the following. Initially the current decreases quickly because the substrate in the reactor is consumed by the anodic reaction which is continuously reducing the substrate concentration. As explained above, new substrate was added at the end of the preceding cycles after the current had dropped; shortly after adding the substrate, the current increased rapidly. Therefore we assume that the reaction rate is strongly concentration dependent at the end of the batch cycle when current is low. With decreasing current also the $CO_2$ signal decreases continuously. The sudden drop in current and ion current after 19 h at point *b* was caused by defective electrode contact which was fixed shortly after. From 31 h to 100 h, the current decreases very slowly from 12 µA to 7.5 µA at 100 h with some fluctuations overlaying the downward trend. At all times, the ion current follows the electrical current.

In Fig. 2, a magnified view of the current and ion current between 85 and 93 h is shown. It reveals that the sensitivity of the DEMS for $CO_2$ is remarkably high: at 85.5 h, for example, the current briefly decreases from 12.3 to 11.8 µA and a change is visible in the ion current signal. This difference of 0.5 µA corresponds to a difference in $CO_2$ production rate of $6.5 \cdot 10^{-13}$ mol/s assuming complete oxidation of acetate to $CO_2$. To attain a similar sensitivity by bubbling $N_2$, for example at 50 ml/min, and analysing the off-gas, it would be necessary to detect 0.02 ppm of $CO_2$ which might be difficult when using for example purity N5 nitrogen that already contains 10 ppm of unspecified gases. Additionally, stripping $CO_2$ from a buffered solution is a very slow process and from literature [11] a time constant in the order of 3000 s can be estimated. As will be shown below, our method allows much faster response times.

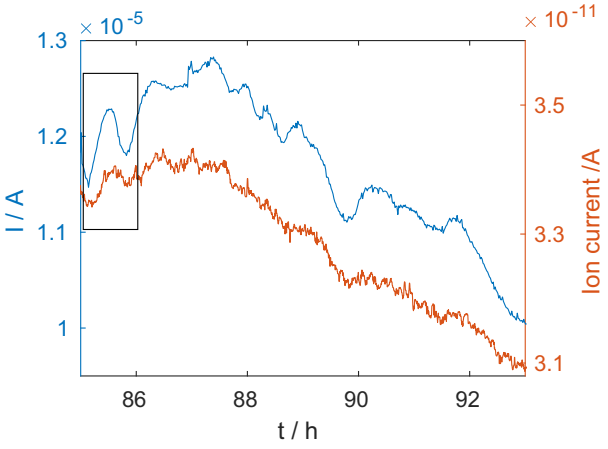


**Fig. 2.** Current and MS signal over time from hour 85 to hour 93 at 0.2 V, showing that changes in current of 0.5 µA corresponding to a difference in $CO_2$ production rate of $6.5 \cdot 10^{-13}$ mol/s cause an observable difference in ion current. Magnified view from Fig. 1. Ion current is potted in orange, electrode current in blue. (For interpretation of the references to color in this figure legend, the reader is referred to the web version of this article.)

When the electrode is situated closely to the porous membrane, which is the case in our set-up, the reaction could be affected by evaporation and subsequent depletion of the reactants [15,17]. However, in a buffered solution at pH 7, the dissociation of acetic acid (pKs = 4.75) is 99.4%, resulting in a negligible evaporation rate. Furthermore, the cell was connected to the mass spectrometer and the vacuum system only in the third batch cycle. Current densities recorded under turnover conditions as well as peak positions in the non-turnover CV with the MS connected, both very closely resemble those without the MS connected. We conclude that the measurement setup does not significantly influence the metabolic activity of the biofilm. Consistent with the considerations above, we did not detect a signal from acetic acid against the background.

Thus the setup is suitable for in-depth analysis of electrochemically active biofilms.

### 3.2. Cyclic voltammetry

In Fig. 3, the MSCV recorded at turnover conditions (labeled 'a' in Fig. 1) is shown. The current exhibits a typical s-shape with a single point of inflection at −0.337 V and a half saturation potential of −0.320 V. The inflection point is very close to a previously reported value for a pure culture *Geobacter sulfurreducens* biofilm of −0.335 V [4]. The ion current follows the current, but a significant time delay can be observed. From the hysteresis between positive and negative scan of approximately 0.12 V and the scan rate of $1\,mVs^{-1}$, a delay of 60 s can be calculated. This delay is larger than in DEMS experiments with anorganic catalysts which can be as low as 0.1 s [15]. In our previous study on CO oxidation in the same cell it was 1–2 s. This increased response time may be attributed to the following differences between the electrodes: The biofilm electrode is thicker than a typical catalyst layer and the transport of $CO_2$ through the inner and outer cell membranes is slower than desorption of a reaction product from a catalyst surface. All in all, the shape of the MSCV under turnover conditions is as expected.

In total, six MSCVs were recorded under substrate depletion conditions: A first CV was recorded at 1 mV/s at hour 26 (see arrow *c* in Fig. 1) after the current had dropped to 12 µA. After that the cell was in open circuit condition for 6 h before potential was applied again (*d* to *e*). At hour 62 (*f*), a second CV was recorded at 1 mV/s. Finally, CVs three to six were recorded at hour 96 at scan rates of 0.5, 1, 2, and 5 mV/s (*g*).

In Fig. 4 the third MSCV, which was recorded at a scan rate of 0.5 mV/s, is depicted. MSCVs 4–6, which were recorded at higher scan rates are given in Figs. S4–S5 in the Supporting information. In the current signal of the positive scan, a shoulder at −0.415 V, a peak at −0.339 V, a second shoulder at −0.290 V and a second peak at −0.195 V can be distinguished. At higher scan rates, the first shoulder disappears and the second one develops into another peak. From these three peaks of the positive scan and the corresponding peaks and shoulders in the negative scan, three formal potentials can be derived: $E_{f,1} = -0.367$ V, $E_{f,2} = -0.307$ V, and $E_{f,3} = -0.205$ V. The first two formal potentials are very close to those of the two major redox systems reported in [4] for *Geobacter sulfurreducens* consistent with this species contributing significantly to the biofilm.

In all MSCVs under substrate depletion conditions, we observed $CO_2$ production. Therefore we will refer to them as low-turnover CVs, rather than non-turnover CVs in the following. $CO_2$ production does not follow the current closely in the low-turnover CVs, and a number of noteworthy features can be observed in Fig. 4:

First, in the negative scan, the current becomes negative below −0.2 V whereas the ion current remains nearly unchanged until reaching the first formal potential of −0.367 V. This phenomenon cannot be explained by a time lag in the detection of $CO_2$ alone: The potential difference between the falling and the rising $CO_2$ signal around −0.39 V is 35 mV. From this value and the scan rate, a time lag of approximately 35 s can be estimated assuming the same delay for the rising and the falling signal. The same delay is obtained from CV four recorded at the double scan rate of 1 mV/s (Fig. S3 in the Supporting information). It corresponds to a potential shift between current and ion current of 17.5 mV at 0.5 mV/s. Thus, $CO_2$ production must continue at an unchanged rate down to a potential near $E_{f,1}$ even though the total current becomes negative at −0.2 V. Also from the shape of the curve we can exclude that the negative current

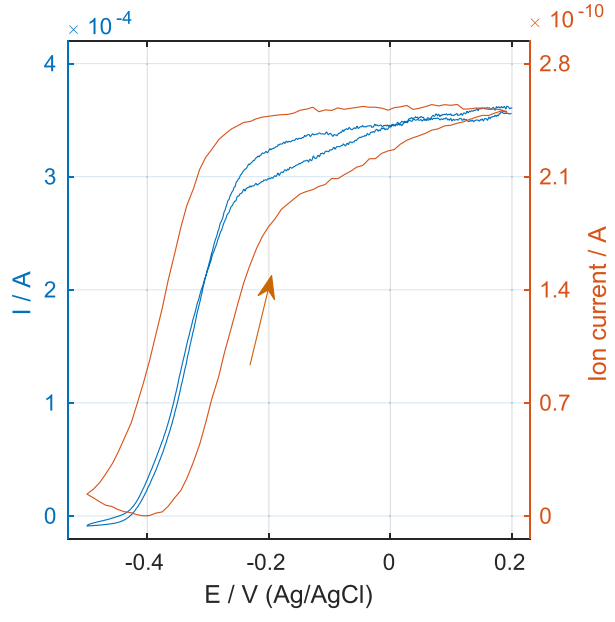


**Fig. 3.** MSCV of the biofilm under turnover conditions at 1 mV/s showing a typical s-shape and a high correlation of current and ion current. Ion current is potted in orange, electrode current in blue. (For interpretation of the references to color in this figure legend, the reader is referred to the web version of this article.)

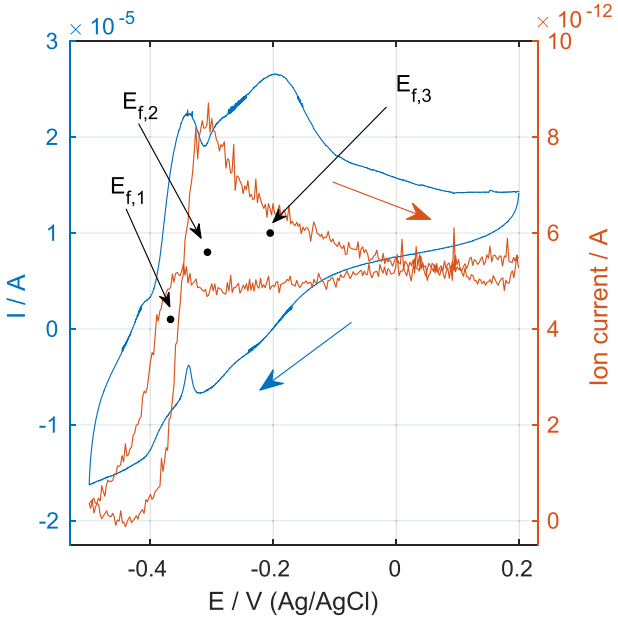


**Fig. 4.** MSCV of the biofilm under low-turnover conditions at 0.5 mV/s. Second cycle of the third low-turnover CV from Fig. 1. Ion current is potted in orange, electrode current in blue. (For interpretation of the references to color in this figure legend, the reader is referred to the web version of this article.)

results from double layer charging. This means that some components in the ARB must be accepting electrons from the electrode and from acetate metabolism at the same time. This observation is in line with literature where it was shown that the observable high capacitance of electroactive biofilms results from a large number of c-type cytochromes undergoing redox reactions [23].

We would like to point out that if the $CO_2$ production resulted from respiration with trace oxygen in the solution, the ion current would be independent of the potential. Thus the presence of oxygen or other chemical electron acceptors can be excluded as an explanation of this phenomenon. Another reason might be that the cells increase the level of NADH or other reduced components inside the cytoplasm [24]. Continued $CO_2$ production coupled with NADH accumulation in the cell seems unlikely though, because of the steep decline in $CO_2$ production below $E_{f,1}$ that appears at various scan rates. If the electrons from acetate oxidation were taken up by a storage mechanism that is not directly coupled to the electrode potential, such as NADH accumulation, it could be expected that the $CO_2$ production would drop at more cathodic potentials for higher scan rates: the saturation of such a storage is basically a function of time and at higher scan rates a more negative potential would be reached before no more electrons can be accepted. This is not the case. The potential where the $CO_2$ production begins to drop does not show a clear trend between 0.5 and 5 mV/s and lies between −0.366 and −0.382 V.

A second feature is observed at −0.35 V in the negative scan: here the ion current rises and reaches a maximum just before dropping. This shows clearly that there are two competing reaction pathways because a single rate limiting electron transfer process cannot account for $CO_2$ production rising with decreasing potential.

As the $CO_2$ signal shows a positive peak at −0.35 V, the first oxidation pathways seems to be triggered at low potential, and is not active at high potentials in parallel with the second pathways that is active in the high potential region. The potential range of the peak in $CO_2$ production suggests that the redox system at $E_{f,1} = -0.367$ V is involved in the low-potential pathway. The high-potential pathways lies in the potential range of the redox system with a formal potential of $E_{f,2}$. The existence of two or even more electron transfer pathways has already been suggested in literature [6,25,26] for pure cultures of *Geobacter sulfurreducens*. Also, in the potential range of $E_{f,1}$ a low potential electron transfer process has been postulated by [5]. In our recent study employing in-situ autofluorescence spectroelectrochemistry [18], it was found that the peak in electrical current in the negative scan, which is also visible in our data at −0.338 V in Fig. 4, does not only result from a decrease in reduction rate but from an oxidative process. The observed increase in $CO_2$ production is thus consistent with these previous results. It is nevertheless quite remarkable, considering that the oxidation rate is already strongly limited by substrate availability under low-turnover conditions. However, even at substrate limiting conditions, the substrate concentration does not reach zero. This is evident from the fact that biological reaction rates or growth rates, for example expressed by Michaelis-Menten or Monod-kinetics ($q = q_{max} \cdot c/(c + K_S)$), decrease with decreasing substrate concentration $c$. The low potential pathway seems to allow the cell to oxidise more substrate at −0.35 V than at higher potentials which usually foster faster oxidation rates. A possible explanation for this might be different half-saturation rate constants $K_S$ of the two pathways. In [27] it was shown that a lower half-saturation rate constant $K_S$ might be associated with a higher energy gain per molecule of substrate. Still, further research efforts are needed to clearly identify the two processes.

Third, the onset potential of $CO_2$ production is discussed. It can be determined from the positive scan. The ion current begins to rise slowly at −0.42 V. When subtracting a 35 mV shift for the lag of the $CO_2$ signal, that was discussed above, there is only a difference of 22 mV between the onset potential of $CO_2$ production and the standard electrode potential of acetate oxidation of −0.477 V [28]. This difference might result from a concentration over potential: according to the Nernst equation, low acetate concentrations in the biofilm shift the equilibrium potential further upwards (see Supporting information for calculations). Recently a study conducted by Peng et al. [29] also found that an established biofilm still produces current close to the standard potential. The very sharp rise and decline of the $CO_2$ signal indicates that even though the biofilm consists of a mixed culture, either one species is dominating the biofilm or all species are using a similar electron transfer mechanism.

Fourth, further on in the positive scan, the ion current peaks near −0.3 V at a level that is much higher than the average ion current. This overshooting is remarkable because it indicates a mechanism for the release of substrate from a storage and will be discussed in detail in the next section. Despite of the presence of another current peak, the ion current continuously falls after the peak. The redox system with a formal potential of −0.205 V thus does not seem to be active for the complete oxidation of acetate to $CO_2$ under these conditions. CVs from a control experiment are shown in Section SI5 in the Supporting information.

### 3.3. Quantitative analysis of $CO_2$ production

A great advantage of mass spectrometry is the fact that it is a quantitative technique. In the following we quantitatively correlate current and ion current, i.e. $CO_2$ production. Quantifying $CO_2$ production rates allows to calculate the share of current resulting from substrate oxidation to $CO_2$ and the share of current resulting from other processes that do not cause $CO_2$ production such as double layer charging, incomplete substrate oxidation or oxidation of other substances. In Fig. 5, the MS signal is plotted over the current recorded in the first 30 h of the CA measurement where a rapid depletion of substrate takes place. It can be seen that there is a linear relationship between current and $CO_2$ production. From the slope of the regression curve, a calibration constant for $CO_2$ is obtained: the amount of $CO_2$ produced can be calculated directly from the current and correlated to the ion current since acetate is the only available substrate and thought to be fully oxidised. For our system, the calibration constant relating the mass spectrometer signal to the production rate of $CO_2$ is $K_{cal} = 0.223 \text{Cmol}^{-1}$. A collection efficiency of 41% was calculated from this value and the MS calibration constant for $CO_2$ of $0.54 \text{Cmol}^{-1}$ as described in [17].

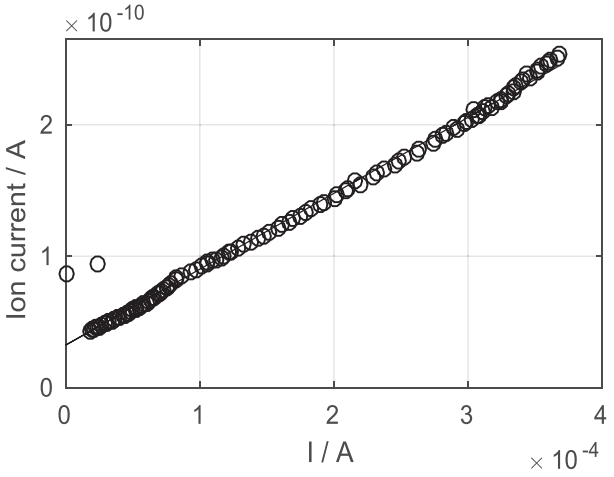


**Fig. 5.** Calibration curve recorded during transition from turnover to non-turnover conditions (hours 10–30 in Fig. 1) showing a linear correlation between current and ion current. Data points are plotted as circles. The continuous line is a linear regression function with $R^2 = 0.99$.

The intercept of the curve with the y-axis is slightly above zero due to the background of the vacuum system. Changing background currents have already been reported in earlier DEMS studies with a shorter duration [30] and it is common practice to use background-subtracted spectra. In Section SI1 in the Supporting information, details on the background subtraction are given.

Since $CO_2$ is produced in the low-turnover CV, it is to be expected that the time averaged current is positive. If acetate oxidation to $CO_2$ is the only irreversible reaction taking place, the amount of $CO_2$ produced calculated by Faraday's law ($CO_2$ with $z = 8$) must be the same as the amount of $CO_2$ detected by the MS $CO_2$. In Table 1, mean values of $CO_2$ production calculated from the current and from the ion current are summarized for all four scan rates. Please note that no error ranges were calculated and the accuracy of the measurements is less than three digits imply. The mean current is not influenced by the scan rate, and the $CO_2$ production calculated from the MS signal in all cases matches the one calculated by Faraday's law. This means that acetate oxidation to $CO_2$ was the only irreversible process in the CV, and reduction and oxidation of cellular redox systems was fully reversible. The agreement of current and ion current allows to rule out contributions from hydrogen recycling from the counter electrode [31]. Also, no hydrogen was detected by the MS in the experiment.

These results strongly suggest that in any non-turnover CV where a positive average current density prevails when integrating over the whole CV, some acetate is still left and oxidised during the CV. The average current density can then be used to quantify the rate of irreversible substrate electro-oxidation. Quite remarkably, many of the "non-turnover" CVs reported in literature are actually low-turnover CVs, for instance in Rimboud et al. [7]. Our findings suggest that the approximate ratio of reversible and irreversible oxidation currents can be estimated even without a DEMS setup.

### 3.4. Storage mechanisms

In [32] it is reported that substrate is stored by a biofilm in an MFC at high substrate concentrations and oxidised later, under substrate depletion conditions. The study suggests that substrate is stored in shape of storage polymers such as poly-$\beta$-hydroxyalkanoates. In this section we show that significant storage also occurs when the electrode potential is too low for immediate substrate oxidation.

To investigate storage capabilities, potential steps were applied and current and ion current were recorded. The potential was stepped from 0.2 V, where electro-oxidation of acetate takes place, to −0.5 V, where no acetate electro-oxidation takes place. Then it was held at −0.5 V for a period of 5, 10 and 30 min to estimate how much substrate or storage compound was stored over time while no oxidation took place. After the respective holding time, the potential was set to 0.2 V again. In Fig. 6, current and ion current over time are depicted for these potential steps. As expected, the ion current drops rapidly after each step to −0.5 V. After stepping the potential back to 0.2 V, the ion current exhibits peaks that increase in size with the length of the preceding period of low potential. These peaks result from the oxidation of stored substances that were produced

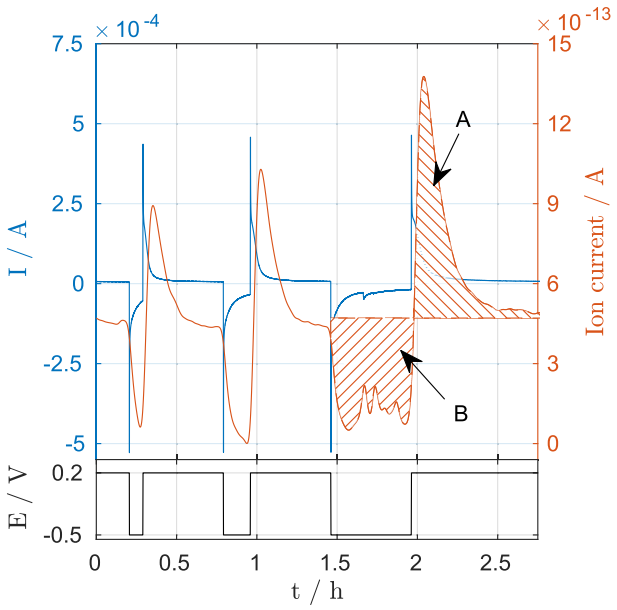


**Fig. 6.** Current and ion current upon stepping the potential from 0.2 to −0.5 V for 5, 10 and 30 min under low-turnover conditions. Arrows A and B indicate integrals above and below baseline for a step duration of 30 min. Ion current is potted in orange, electrode current in blue. (For interpretation of the references to color in this figure legend, the reader is referred to the web version of this article.)

during low potential when no oxidation took place. When comparing the integrals of the ion current during the time at −0.5 V and the integral of the peak after switching back to 0.2 V, the storage efficiency can be estimated. Arrows A and B in Fig. 6 show these integrals exemplarily for the last potential step. In Fig. 7, the integrals of the ion current peaks are plotted over the duration of the preceding period at low potential as red circular markers. The marker indicated by arrow A in Fig. 7 corresponds to the integral area A in Fig. 6. The other points were obtained in the same manner. The peak area increases linearly with the duration of the preceding low potential period, indicating that the storage rate was constant during all three steps. The linear relationship suggests that only a small part of the storage capacity is used even after 30 min. Acetate replenishment is not the reason for the observed behaviour: From the recirculation flow rate and the cell volume a hydraulic retention time of 44 s can be calculated. Acetate concentration would reach an equilibrium within a time much shorter than the 30 min of the last potential step experiment and thus cannot explain the experimental data. The linear relationship in Fig. 6 shows that acetate replenishment does not play a significant role for the shorter steps of 5 and 10 min either.

Also in Fig. 7, the integrals of ion current below the baseline during the period at low potential are plotted with blue cross markers. The marker indicated by arrow B corresponds to the integral area B. These integrals match the integrals of the peaks very well. This confirms that all substrate not oxidised at low potential is stored

**Table 1**
Average current, ion current (background corrected), and $CO_2$ production rates during low-turnover CVs at different scan rates. The values do not deviate significantly from current and ion current during CA measurement right before the CVs.

| Scan rate | Mean current | $CO_2$ from current | Mean ion current | $CO_2$ from ion current |
|---|---|---|---|---|
| 0.5 mV/s | 7.78 µA | $2.02 \cdot 10^{-11}$ mol s$^{-1}$ | 4.71 pA | $2.11 \cdot 10^{-11}$ mol s$^{-1}$ |
| 1 mV/s | 7.77 µA | $2.01 \cdot 10^{-11}$ mol s$^{-1}$ | 4.78 pA | $2.14 \cdot 10^{-11}$ mol s$^{-1}$ |
| 2 mV/s | 7.77 µA | $2.01 \cdot 10^{-11}$ mol s$^{-1}$ | 4.69 pA | $2.10 \cdot 10^{-11}$ mol s$^{-1}$ |
| 5 mV/s | 7.40 µA | $1.92 \cdot 10^{-11}$ mol s$^{-1}$ | 4.62 pA | $2.07 \cdot 10^{-11}$ mol s$^{-1}$ |

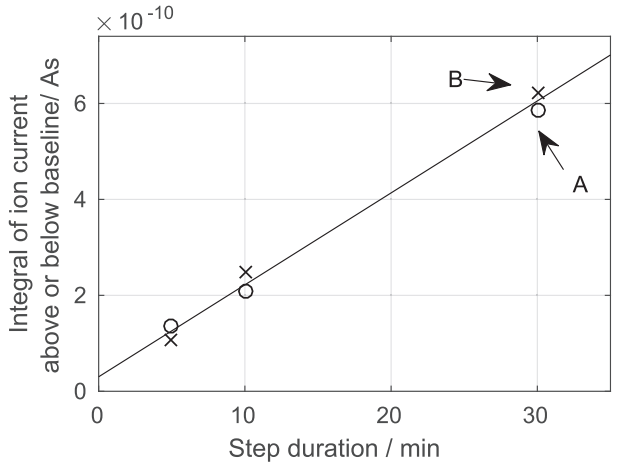


**Fig. 7.** Absolute values of the integrals of ion current below the baseline at −0.5 V and integrals of ion current above the baseline directly after stepping back to 0.2 V over the time for which the potential was set to −0.5 V. Arrows A and B correspond to the areas marked in Fig. 6. Integrals above the baseline are plotted as circles, integrals below baseline as crosses. The continuous line is a linear regression function.

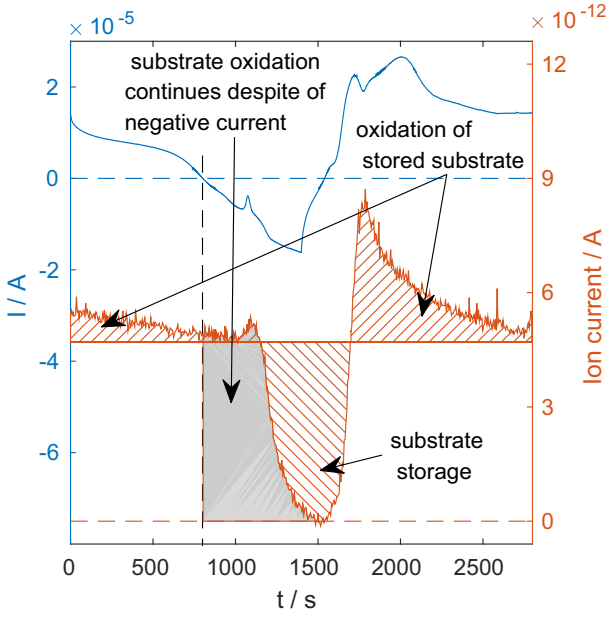


**Fig. 8.** Background corrected ion current over time during MSCV at 0.5 mV/s. The average ion current is approximately the same as the ion current during CA right before the CV. The hatched areas below and above the average line have the same size and are proportional to amount of substrate converted to a storage compound at low potential and oxidised later on at higher potential. Ion current is potted in orange, electrode current in blue. (For interpretation of the references to color in this figure legend, the reader is referred to the web version of this article.)

and oxidised at high potential. From the current signal, the storage cannot be deduced directly because of the large capacitive currents that cause a negative current after the steps to −0.5 V. The same measurement was performed under turnover conditions. The respective figures can be found in Figs. S10 and S11 in the Supporting information. Under turnover conditions, also storage can be observed and the amount of storage compound formed still increases linearly with the duration of the low potential period. However, not all substrate that is not oxidised during low potential is converted to a storage compound. The peak area after the positive potential step is only 20% of the area below the baseline during low potential, indicating that the maximum rate of substrate storage is only one-fifth of the maximum rate of substrate electro-oxidation. This rate remains constant for 30 min indicating that again only a small part of the storage capacity is utilized.

The potential dependency of the substrate storage can be observed in the MSCV. Actually, two storage mechanisms are visible in the MSCVs which will be discussed further in the following: a) substrate storage and b) charge storage.

In the low-turnover CV in Fig. 4, $CO_2$ production diminishes at low potentials whereas a large peak can be observed in the positive scan. The average currents and $CO_2$ production rates over the whole CV, however, approximately equal the values during CA measurements. In Table 1, the average currents and $CO_2$ production rates over the CV are reported for all scan rates. Considering that the oxidation rate during CA is limited by substrate availability, the average oxidation rate during the CVs can only be identical to that rate if - just like in the potential step experiments at low substrate availability - all the substrate that is not oxidised in the low potential region is stored as a storage compound and completely oxidised in the high potential region. Table 1 also shows that the amount of $CO_2$ detected by the MS equals the amount of $CO_2$ calculated from the Faraday current with four electrons transferred per molecule of $CO_2$ for all CV scan rates. If substances other than acetate or a storage compound synthesized from acetate were oxidised, it is very likely that a different number of electrons per molecule would be transferred. Also it would be difficult to imagine a mechanism that causes the biofilm to metabolize exactly the amount of energy reserves that compensates for reduced acetate oxidation at low potential at four different scan rates.

The storage is visualized in Fig. 8 by plotting current and ion current over time during the MSCV at 0.5 mV $s^{-1}$. Substrate is stored between 1115 s and 1700 s. Similarly as for the CA measurements, integrals of $CO_2$ production allow to estimate the amount of acetate equivalent that is stored by integrating the ion current above and below the baseline. In Fig. 8 both areas are indicated by arrows. Because a part of the storage compound is oxidised only in the following cycle of the CV, the area corresponding to oxidation of stored substrate is split into two parts.

Using the calibration constant that was defined above, it can be calculated that $4.26 \cdot 10^{-9}$mol of acetate equivalent are stored. At the higher scan rates, the amount of storage is lower because the period of time where the potential is too low for substrate oxidation is shorter. The formation of the storage substance does not go along with $CO_2$ production. At high potentials it is completely oxidised to $CO_2$. In [2] it is hypothesized that ARB could continue substrate breakdown under production of NADH in absence of an extracellular electron acceptor. This step, however, goes hand in hand with $CO_2$ production. As we observe no $CO_2$ production at very low electrode potentials there must exist another mechanism that takes up acetate without liberation of $CO_2$. This is consistent with results from Song et al. [33] who reported that the citric acid circle in *Geobacter sulfurreducens* is regulated down at lower current densities. The accumulation of storage polymers as suggested in [32] seems more likely considering our data because, for instance, the transformation of acetate via Acetyl-CoA and Acetoacetyl-CoA to PHB would not release $CO_2$. Elucidating the exact nature of the storage mechanism is out of scope of this work as it needs further refined analysis.

Charge storage occurs after 800 s when the current begins to flow in cathodic direction. The grey area under the ion current curve represents the amount of $CO_2$ that is produced despite of a cathodic current. During this time, electrons from acetate oxidation and from the cathodic electrode current must be stored in the biofilm. From the integral of current (5.86 mC), which corresponds to stored $e^-$, and of $CO_2$ production (3.81 mC), which would release $e^-$ as well, a total charge storage capacity of 9.67 mC can be calculated.

## 4. Conclusions

In this work, it was shown that DEMS constitutes a valuable technique for analysing biofilms of electrode respiring bacteria in-vivo and online. We demonstrated how to gain insights into the coupling of extracellular electron transfer and metabolic activity: MSCVs were recorded under turnover and under substrate depletion conditions. The onset of complete oxidation of acetate to $CO_2$ is a few mV above the equilibrium potential. Two competing extracellular electron transfer mechanisms have been directly identified in low-turnover CVs, the first one is active at potentials greater than 0.35 V, the second one below that potential. Furthermore, the existence of two significant storage mechanisms has been shown: 1) A charge storage mechanism that allows substrate oxidation to proceed at a constant rate despite of current flowing in cathodic direction during the negative scan of the low-turnover CV. 2) A carbon storage mechanism that allows the biofilm to take up acetate at an unchanged rate even though the oxidation to $CO_2$ stops at very low potentials. Whereas this work lays a basis for quantitative analysis of substrate storage mechanisms, many more questions are open concerning the factors that determine these processes. It was observed that the storage process does not cause $CO_2$ production. When the potential is too low to allow oxidation of acetate, at low substrate availability, all substrate that is not oxidised is stored in the biofilm. When the potential is too low to allow oxidation of acetate, at high substrate availability, the storage rate was observed to be 20% of the substrate oxidation rate at high potential. Our results suggest that, under certain dynamic conditions, charge transfer is only loosely connected to acetate consumption and $CO_2$ production. This is an important fact to be further explored and to be considered when evaluating dynamic electrochemical measurements such as CV or EIS. A better understanding of factors that influence storage capacities might also enable a more flexible operation of bioelectrochemical cells to meet requirements of fluctuating energy demands.

## Acknowledgments

This research did not receive any specific grant from funding agencies in the public, commercial, or not-for-profit sectors. We would like to thank Jonas Perk for performing some of the measurements.

## Appendix A. Supplementary data

Supplementary data to this article can be found online at https://doi.org/10.1016/j.bioelechem.2018.01.014.

## References

[1] F. Harnisch, K. Rabaey, The diversity of techniques to study electrochemically active biofilms highlights the need for standardization, ChemSusChem 5 (6) (2012) 1027–1038. https://doi.org/10.1002/cssc.201100817.
[2] N.D. Rose, J.M. Regan, Changes in phosphorylation of adenosine phosphate and redox state of nicotinamide-adenine dinucleotide (phosphate) in *Geobacter sulfurreducens* in response to electron acceptor and anode potential variation, Bioelectrochemistry 106 (2015) 213–220. https://doi.org/10.1016/j.bioelechem.2015.03.003.
[3] U. Krewer, T. Vidakovic-Koch, L. Rihko-Struckmann, Electrochemical oxidation of carbon-containing fuels and their dynamics in low-temperature fuel cells, ChemPhysChem 12 (14) (2011) 2518–2544. https://doi.org/10.1002/cphc.201100095.
[4] K. Fricke, F. Harnisch, U. Schröder, On the use of cyclic voltammetry for the study of anodic electron transfer in microbial fuel cells, Energy & Environmental Science 1 (1) (2008) 144. https://doi.org/10.1039/b802363h.
[5] L. Zacharoff, C.H. Chan, D.R. Bond, Reduction of low potential electron acceptors requires the CbcL inner membrane cytochrome of *Geobacter sulfurreducens*, Bioelectrochemistry 107 (2016) 7–13. https://doi.org/10.1016/j.bioelechem.2015.08.003.
[6] R.A. Yoho, S.C. Popat, C.I. Torres, Dynamic potential-dependent electron transport pathway shifts in anode biofilms of *Geobacter sulfurreducens*, ChemSusChem 7 (12) (2014) 3413–3419. https://doi.org/10.1002/cssc.201402589.
[7] M. Rimboud, E. Desmond-Le Quemener, B. Erable, T. Bouchez, A. Bergel, Multi-system Nernst-Michaelis-Menten model applied to bioanodes formed from sewage sludge, Bioresour. Technol. 195 (2015) 162–169. https://doi.org/10.1016/j.biortech.2015.05.069.
[8] P.A. Selembo, J.M. Perez, W.A. Lloyd, B.E. Logan, High hydrogen production from glycerol or glucose by electrohydrogenesis using microbial electrolysis cells, Int. J. Hydrog. Energy 34 (13) (2009) 5373–5381. https://doi.org/10.1016/j.ijhydene.2009.05.002.
[9] N. Montpart, L. Rago, J.A. Baeza, A. Guisasola, Hydrogen production in single chamber microbial electrolysis cells with different complex substrates, Water Res. 68 (2015) 601–615. https://doi.org/10.1016/j.watres.2014.10.026.
[10] J. Yu, Y. Park, T. Lee, Electron flux and microbial community in microbial fuel cells (open-circuit and closed-circuit modes) and fermentation, J. Ind. Microbiol. Biotechnol. 42 (7) (2015) 979–983. https://doi.org/10.1007/s10295-015-1629-2.
[11] A.Z. Andersen, F.R. Lauritsen, L.F. Olsen, On-line monitoring of $CO_2$ production in *Lactococcus lactis* during physiological pH decrease using membrane inlet mass spectrometry with dynamic pH calibration, Biotechnol. Bioeng. 92 (6) (2005) 740–747. https://doi.org/10.1002/bit.20641.
[12] M.J. Hayward, T. Kotiaho, A.K. Lister, R.G. Cooks, G.D. Austin, R. Narayan, G.T. Tsao, On-line monitoring of bioreactions of *Bacillus polymyxa* and *Klebsiella oxytoca* by membrane introduction tandem mass spectrometry with flow injection analysis sampling, Anal. Chem. 62 (17) (1990) 1798–1804. https://doi.org/10.1021/ac00216a014.
[13] F.R. Lauritsen, L.T. Nielsen, H. Degn, D. Lloyd, S. Bohátka, Identification of dissolved volatile metabolites in microbial cultures by membrane inlet tandem mass spectrometry, Biol. Mass Spectrom. 20 (5) (1991) 253–258. https://doi.org/10.1002/bms.1200200504.
[14] J. Das, H. Timm, H.-G. Busse, H. Degn, Oscillatory $CO_2$ evolution in glycolysing yeast extracts, Yeast 6 (3) (1990) 255–261. https://doi.org/10.1002/yea.320060310.
[15] H. Baltruschat, Differential electrochemical mass spectrometry, J. Am. Soc. Mass Spectrom. 15 (12) (2004) 1693–1706. http://link.springer.com/. https://doi.org/10.1016/j.jasms.2004.09.011.
[16] A.-E.-A.A. Abd-El-Latif, C. Bondue, S. Ernst, M. Hegemann, J. Kaul, M. Khodayari, E. Mostafa, A. Stefanova, H. Baltruschat, Insights into electrochemical reactions by differential electrochemical mass spectrometry, TrAC Trends Anal. Chem. 70 (2015) 4–13. https://doi.org/10.1016/j.trac.2015.01.015.
[17] F. Kubannek, U. Krewer, A cyclone flow cell for quantitative analysis of kinetics at porous electrodes by differential electrochemical mass spectrometry, Electrochim. Acta 210 (2016) 862–873. https://doi.org/10.1016/j.electacta.2016.05.212.
[18] I. Schmidt, A. Pieper, H. Wichmann, B. Bunk, K. Huber, J. Overmann, P.J. Walla, U. Schröder, In Situ Autofluorescence Spectroelectrochemistry for the Study of Microbial Extracellular Electron Transfer, ChemElectroChem 4 (10) (2017) 2515–2519. https://doi.org/10.1002/celc.201700675.
[19] C.I. Torres, A.K. Marcus, P. Parameswaran, B.E. Rittmann, Kinetic experiments for evaluating the Nernst-Monod model for anode-respiring bacteria (ARB) in a biofilm anode, Environ. Sci. Technol. 42 (17) (2008) 6593–6597. https://doi.org/10.1021/es800970w.
[20] D. Millo, F. Harnisch, S.A. Patil, H.K. Ly, U. Schröder, P. Hildebrandt, In situ spectroelectrochemical investigation of electrocatalytic microbial biofilms by surface-enhanced resonance Raman spectroscopy, Angew. Chem. Int. Ed. 50 (11) (2011) 2625–2627. https://doi.org/10.1002/anie.201006046.
[21] J.R. Kim, B. Min, B.E. Logan, Evaluation of procedures to acclimate a microbial fuel cell for electricity production, Appl. Microbiol. Biotechnol. 68 (1) (2005) 23–30. https://doi.org/10.1007/s00253-004-1845-6.
[22] W.E. Balch, G.E. Fox, L.J. Magrum, C.R. Woese, R.S. Wolfe, Methanogens: reevaluation of a unique biological group, Microbiol. Rev. 43 (2) (1979) 260–296. https://doi.org/10.1016/j.watres.2010.10.010.
[23] N.S. Malvankar, T. Mester, M.T. Tuominen, D.R. Lovley, Supercapacitors based on c-type cytochromes using conductive nanostructured networks of living bacteria, ChemPhysChem 13 (2) (2012) 463–468. https://doi.org/10.1002/cphc.201100865.
[24] R. Kumar, L. Singh, A. Zularisam, Exoelectrogens: recent advances in molecular drivers involved in extracellular electron transfer and strategies used to improve it for microbial fuel cell applications, Renew. Sust. Energ. Rev. 56 (2016) 1322–1336. https://doi.org/10.1016/j.rser.2015.12.029.
[25] C.E. Levar, C.L. Hoffman, A.J. Dunshee, B.M. Toner, D.R. Bond, Redox potential as a master variable controlling pathways of metal reduction by *Geobacter sulfurreducens*, ISME J. 11 (3) (2017) 741–752. https://doi.org/10.1038/ismej.2016.146.
[26] A.S. Commault, G. Lear, M.A. Packer, R.J. Weld, Influence of anode potentials on selection of *Geobacter* strains in microbial electrolysis cells, Bioresour. Technol. 139 (2013) 226–234. https://doi.org/10.1016/j.biortech.2013.04.047.
[27] Y. Liu, Y.-M. Lin, S.-F. Yang, A thermodynamic interpretation of the Monod equation, Curr. Microbiol. 46 (3) (2003) 233–234. https://doi.org/10.1007/s00284-002-3934-z.
[28] Z. He, L.T. Angenent, Application of bacterial biocathodes in microbial fuel cells, Electroanalysis 18 (19–20) (2006) 2009–2015. https://doi.org/10.1002/elan.200603628.

[29] L. Peng, X.-T. Zhang, J. Yin, S.-Y. Xu, Y. Zhang, D.-T. Xie, Z.-L. Li, *Geobacter sulfurreducens* adapts to low electrode potential for extracellular electron transfer, Electrochim. Acta 191 (2016) 743–749. https://doi.org/10.1016/j.electacta.2016.01.033.

[30] C. Bondue, A.-E.-A.A. Abd-El-Latif, P. Hegemann, H. Baltruschat, Quantitative study for oxygen reduction and evolution in aprotic organic electrolytes at gas diffusion electrodes by DEMS, J. Electrochem. Soc. 162 (3) (2015) A479–A487. https://doi.org/10.1149/2.0871503jes.

[31] H.-S. Lee, B.E. Rittmann, Significance of biological hydrogen oxidation in a continuous single-chamber microbial electrolysis cell, Environ. Sci. Technol. 44 (3) (2010) 948–954. https://doi.org/10.1021/es9025358.

[32] S. Freguia, K. Rabaey, Z. Yuan, J. Keller, Electron and carbon balances in microbial fuel cells reveal temporary bacterial storage behavior during electricity generation, Environ. Sci. Technol. 41 (8) (2007) 2915–2921. http://pubs.acs.org/doi/abs/10.1021/es062611i. https://doi.org/10.1021/es062611i.

[33] J. Song, D. Sasaki, K. Sasaki, S. Kato, A. Kondo, K. Hashimoto, S. Nakanishi, Comprehensive metabolomic analyses of anode-respiring *Geobacter sulfurreducens* cells: the impact of anode-respiration activity on intracellular metabolite levels, Process Biochem. 51 (1) (2016) 34–38. https://doi.org/10.1016/j.procbio.2015.11.012.